

Chingakham R. Singh,<sup>a</sup> Scott Lovell,<sup>b</sup> Nurjahan Mehzabeen,<sup>b</sup> Wasimul Q. Chowdhury,<sup>a</sup> Eric S. Geanes,<sup>a</sup> Kevin P. Battaile<sup>c</sup> and Jeroen Roelofs<sup>a\*</sup>

<sup>a</sup>Division of Biology, Kansas State University, 338 Ackert Hall, Manhattan, KS 66506, USA,

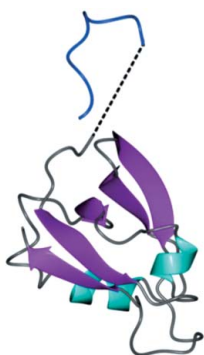
<sup>b</sup>Protein Structure Laboratory, University of Kansas, Del Shankel Structural Biology Center, Lawrence, KS 66047, USA, and <sup>c</sup>IMCA-CAT Hauptman–Woodward Medical Research Institute, 9700 South Cass Avenue, Building 435A, Argonne, IL 60439, USA

Correspondence e-mail: jroelofs@ksu.edu

Received 6 January 2014

Accepted 19 February 2014

**PDB reference:** proteasome-assembly chaperone Nas2 PDZ domain, 4o06



# 1.15 Å resolution structure of the proteasome-assembly chaperone Nas2 PDZ domain

The 26S proteasome is a 2.5 MDa protease dedicated to the degradation of ubiquitinated proteins in eukaryotes. The assembly of this complex containing 66 polypeptides is assisted by at least nine proteasome-specific chaperones. One of these, Nas2, binds to the proteasomal AAA-ATPase subunit Rpt5. The PDZ domain of Nas2 binds to the C-terminal tail of Rpt5; however, it does not require the C-terminus of Rpt5 for binding. Here, the 1.15 Å resolution structure of the PDZ domain of Nas2 is reported. This structure will provide a basis for further insights regarding the structure and function of Nas2 in proteasome assembly.

## 1. Introduction

The eukaryotic proteasome consists of a core particle (CP) and a regulatory particle (RP). The CP is a cylindrically shaped structure with the proteolytic active sites on the inner surface of this complex (Groll *et al.*, 1997). One or both ends can associate with the RP, forming the 26S proteasome. CP assembly and RP assembly are both assisted by proteasome-specific chaperones (Bedford *et al.*, 2010). The RP-specific chaperones Nas6, Nas2, Hsm3 and Rpn14 are important for the assembly of a hetero-hexameric AAA-ATPase ring formed by the subunits Rpt1 to Rpt6 (Funakoshi *et al.*, 2009; Kaneko *et al.*, 2009; Le Tallec *et al.*, 2009; Roelofs *et al.*, 2009; Saeki *et al.*, 2009). Interestingly, each chaperone largely consists of protein–protein interaction motifs: Nas6 contains seven ankyrin repeats, Hsm3 is formed by armadillo/heat-like repeats, Rpn14 contains a WD40 domain and Nas2 has a predicted PDZ domain. Although structurally different, each chaperone binds to the C-domain of a specific Rpt protein. Structural studies looking at the interaction between Nas6 and Rpt3 (Nakamura *et al.*, 2007; Roelofs *et al.*, 2009), Hsm3 and Rpt1 (Barrault *et al.*, 2012; Takagi *et al.*, 2012; Park *et al.*, 2013), and Rpn14 and Rpt6 (Ehlinger *et al.*, 2013) have provided substantial structural insights. However, no structural data for Nas2, or the human ortholog p27/PSMD9, have been published to date. Binding studies between Nas2 and Rpt5 have shown that deletion of the C-terminal residue of Rpt5 did not impact Nas2 binding (Lee *et al.*, 2011). Deletion of the last three amino acids, on the other hand, caused a strong reduction in binding. This indicates that the tail of Rpt5 is important for binding with Nas2 (Lee *et al.*, 2011). This same tail is also involved in the association between the Rpt5 subunit and the CP (Tian *et al.*, 2011; Beck *et al.*, 2012; Lander *et al.*, 2012), which suggests that the binding of Nas2 prevents the association of Rpt5, or Rpt5-containing complexes, with the CP. The structure of the Nas2 PDZ domain reported here is the first step towards a structural understanding of this interaction.

## 2. Materials and methods

### 2.1. Macromolecule production

The open reading frame of *Saccharomyces cerevisiae* Nas2 was subcloned into a pGEX-6P1-derived plasmid, creating plasmid pJR500 (Lee *et al.*, 2011). Based on domain and secondary-structure prediction analyses, two truncated versions of Nas2 containing the single PDZ domain were generated: Nas2LND, covering amino acids

**Table 1**

Amino-acid sequence of the Nas2LND fragment that crystallized.

Source organism	<i>S. cerevisiae</i> strain ATCC 204508/S288c
DNA source	<i>S. cerevisiae</i> strain ATCC 204508/S288c
Expression vector	pGEX-6P1-derived plasmid
Expression host	<i>E. coli</i> BL21(DE3)
Complete amino-acid sequence of the construct produced	GPLTRRASVGSQAIOYTIPIFAFISEVVPGPSDDK-ADIKVDDKLSIGNVHAANHSKLNQIMVV-MKNEDRPLPVLRLREGQILKTSLTSPSRNWNG-RLLGCRIQEL
Vector-derived residues	GPLTRRASVGS

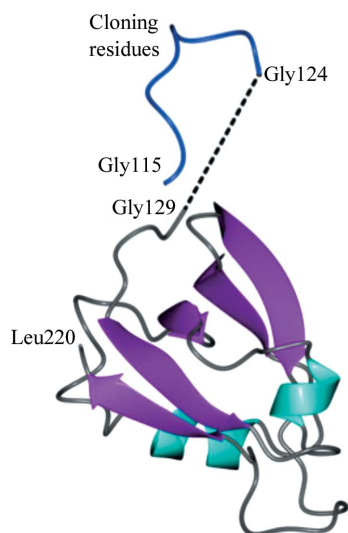
Gln126–Leu220 (pJR607), and Nas2LND, covering Asn91–Leu220 (pJR606). Expression and purification of the different proteins were conducted as described previously for Hsm3 (Park *et al.*, 2013). Basically, *Escherichia coli* cells induced to express the GST-fused proteins were lysed. The fusion proteins were bound to glutathione resin. The affinity tag was removed by incubation with PreScission protease and the eluted proteins were further purified by size-exclusion chromatography using a Superdex 200 (10/300 GL) column.

## 2.2. Crystallization

A purified sample of Nas2LND (Table 1) concentrated to 7.0 mg ml<sup>-1</sup> in 50 mM NaCl, 50 mM Tris–HCl pH 6.8, 1 mM DTT, 1 mM EDTA was used for crystallization screening. All crystallization experiments were conducted by sitting-drop vapor diffusion in Compact Jr plates (Emerald Bio) using equal volumes of protein and crystallization solutions equilibrated against 75 µl of the latter. After two months, prismatic crystals of ~0.2 mm in length were obtained at 4°C from Wizard Classic 4 screen (Emerald Bio) condition No. 26 [10% (w/v) PEG 2000 MME, 100 mM sodium acetate/acetic acid pH 5.5, 200 mM ammonium sulfate].

## 2.3. Data collection and processing

Crystal samples were transferred to a fresh drop composed of 75% crystallization solution and 25% (v/v) PEG 400 and stored in liquid nitrogen. Diffraction data were collected in-house using a Rigaku RU-H3R rotating-anode generator (Cu Kα) equipped with Osmic Blue confocal mirrors and an R-AXIS IV<sup>++</sup> image-plate detector.

**Figure 1**

Structure of the Nas2 PDZ domain. Asymmetric unit of Nas2LND colored by secondary structure: sheet, magenta; helix, cyan. The disordered region is indicated by the dashed line. N-terminal residues resulting from cloning are colored blue.

**Table 2**

Data-collection statistics for Nas2LND refined to 1.15 Å resolution.

Values in parentheses are for the highest resolution shell.	
Unit-cell parameters (Å, °)	$a = 39.97, b = 39.97, c = 115.80,$ $\alpha = \beta = \gamma = 90$
Space group	$P4_12_12$
Resolution (Å)	39.97–1.15 (1.17–1.15)
Wavelength (Å)	1.0000
Temperature (°C)	–173
Observed reflections	808924
Unique reflections	33545
$\langle I/\sigma(I) \rangle$	23.0 (3.4)
Completeness (%)	97.9 (95.1)
Multiplicity	24.1 (17.6)
$R_{\text{merge}}^\dagger$ (%)	7.7 (107.0)
$R_{\text{meas}}^\ddagger$ (%)	7.8 (110.0)
$R_{\text{p.i.m.}}^\ddagger$ (%)	1.6 (25.6)
$CC_{1/2}^\S$	0.999 (0.880)

$^\dagger R_{\text{merge}} = \sum_{hkl} \sum_i |I_i(hkl) - \langle I(hkl) \rangle| / \sum_{hkl} \sum_i I_i(hkl)$ , where  $I_i(hkl)$  is the intensity measured for the  $i$ th reflection and  $\langle I(hkl) \rangle$  is the average intensity of all reflections with indices  $hkl$ .  $^\ddagger R_{\text{meas}}$  is the redundancy-independent (multiplicity-weighted)  $R_{\text{merge}}$  (Evans, 2006, 2011).  $R_{\text{p.i.m.}}$  is the precision-indicating (multiplicity-weighted)  $R_{\text{merge}}$  (Diederichs & Karplus, 1997; Weiss, 2001).  $^\S CC_{1/2}$  is the correlation coefficient of the mean intensities between two random half-sets of data (Karplus & Diederichs, 2012; Evans, 2012).

**Table 3**

Structure refinement.

Refinement	
Resolution (Å)	32.90–1.15
Reflections (working/test)	31796/1698
$R$ factor/ $R_{\text{free}}^\dagger$ (%)	17.2/19.4
No. of atoms (protein/sulfate/PEG/water)	804/5/8/98
Model quality	
R.m.s. deviations	
Bond lengths (Å)	0.012
Bond angles (°)	1.356
Average $B$ factor (Å <sup>2</sup> )	
All atoms	18.0
Protein	16.4
Sulfate	30.6
PEG	29.5
Water	28.8
Coordinate error (maximum likelihood) (Å)	0.12
Ramachandran plot	
Most favored (%)	96.2
Additionally allowed (%)	3.8

$^\dagger R$  factor =  $\sum_{hkl} | |F_{\text{obs}}| - |F_{\text{calc}}| | / \sum_{hkl} |F_{\text{obs}}|$ ;  $R_{\text{free}}$  is calculated in an identical manner using 5% of randomly selected reflections that were not included in the refinement.

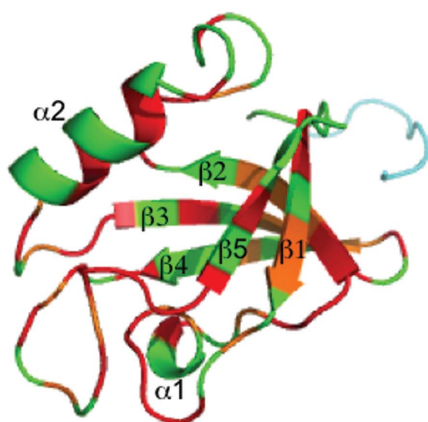
High-resolution data were collected on beamline 17-ID at the Advanced Photon Source using a Dectris Pilatus 6M pixel-array detector. Intensities were integrated using *XDS* (Kabsch, 2010a,b) and Laue class analysis and data scaling was performed with *AIMLESS* (Evans, 2011; Evans & Murshudov, 2013), which indicated that the highest probability Laue class was  $4/mmm$  and the most likely space groups were  $P4_12_12$  or  $P4_32_12$ . Data-collection statistics are given in Table 2.

## 2.4. Structure solution and refinement

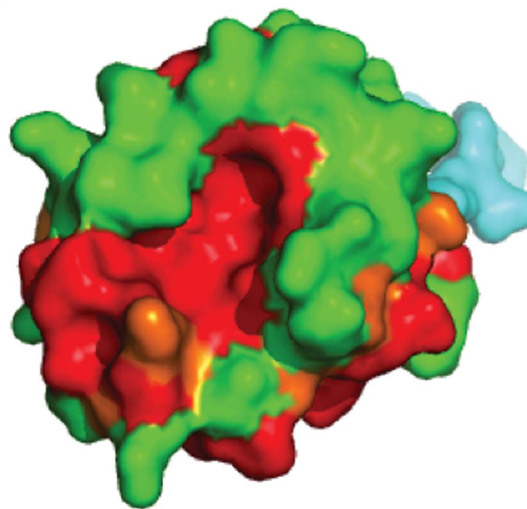
The Matthews coefficient (Matthews, 1968) indicated that the asymmetric unit contained a single molecule ( $V_M = 1.99 \text{ Å}^3 \text{ Da}^{-1}$ , ~40% solvent). Structure solution was conducted by molecular replacement with *BALBES* (Long *et al.*, 2008), in which the top solution was obtained using the GRASP55 GRASP domain (PDB entry 3rle; Truschel *et al.*, 2011) as the search model. Following initial refinement with *PHENIX* (Adams *et al.*, 2010) the  $R$  and  $R_{\text{free}}$  converged at 42.8 and 46.4%, respectively. The model was improved

		$\beta 1$	$\alpha 1$	$\beta 2$	$\alpha 2$	$\beta 3$		
Nas2LND	134	FAFISEVVPGSPDKADIKVDDKLI	SIGNVHAANHSKLN	IQMVMKNE	DRPLPVLLRE		193	
		FA ++ + PGSP+	A ++VDD+++	G+V+	N L NI VV +E +PL V ++R			
PSMD9	136	FAKVNSISPGSPAS	IAGLQVDDEIVEFGSV	NTQNFQSLHN	IGSVVQHSE	GKPLNVTVIRR	195	
		$\beta 4$	$\beta 5$					
Nas2LND	194	GQILKTS	LTSPSRNWN	GRLLGCRIQEL-				220
		G+ + L P+R	W G+LLGC I					
PSMD9	196	GEKHQLRLVP	TR-WAGKLLGC	NIPLQR				223

(a)



(b)



(c)

Figure 2

Mapping residues that are conserved between Nas2 and the human ortholog PSMD9. (a) Alignment of Nas2 PDZ-domain residues with the human ortholog PSMD9. Residues modeled in the crystal structure of Nas2 were used in a *BLASTp* search against the human protein RefSeq database. The top hit was the human ortholog of Nas2, PSMD9, showing 42% identity and 64% conserved residues (the latter are indicated with +). (b) Graphic structure of Nas2 in green. Based on an alignment between Nas2 and PSMD9, conserved residues were colored orange and identical residues red. The cloning-derived residues are in blue. (c) Surface representation of (b). Note the conservation in the groove of the PDZ domain between  $\alpha$ -helix 2 and  $\beta$ -strand 5. In PDZ-domain proteins this region commonly binds peptides/C-termini from their binding partner.

by automated model building with *ARP/wARP* (Langer *et al.*, 2008) and the *R* and *R*<sub>free</sub> converged at 20.7 and 23.5%, respectively, following refinement of this model. To check that the correct space group had been assigned, the model was used for a molecular-replacement search with *Phaser* (McCoy *et al.*, 2007) checking all space groups with 422 point symmetry. The top solution was obtained in space group *P4*<sub>1</sub>2<sub>1</sub>2 (LLG = 13 591) which was used from this point forward. Additional structure refinement and manual model building with the high-resolution synchrotron data were conducted with *PHENIX* and *Coot* (Emsley *et al.*, 2010), respectively. All atoms were refined with anisotropic atomic displacement parameters. H atoms were placed in idealized positions and refined with a riding model. Structure validation was conducted with *MolProbity* (Chen *et al.*, 2010) and figures were prepared using the *CCP4mg* package (McNicholas *et al.*, 2011). Structure-refinement statistics are given in Table 2.

### 3. Results and discussion

#### 3.1. Structure of the Nas2 PDZ domain

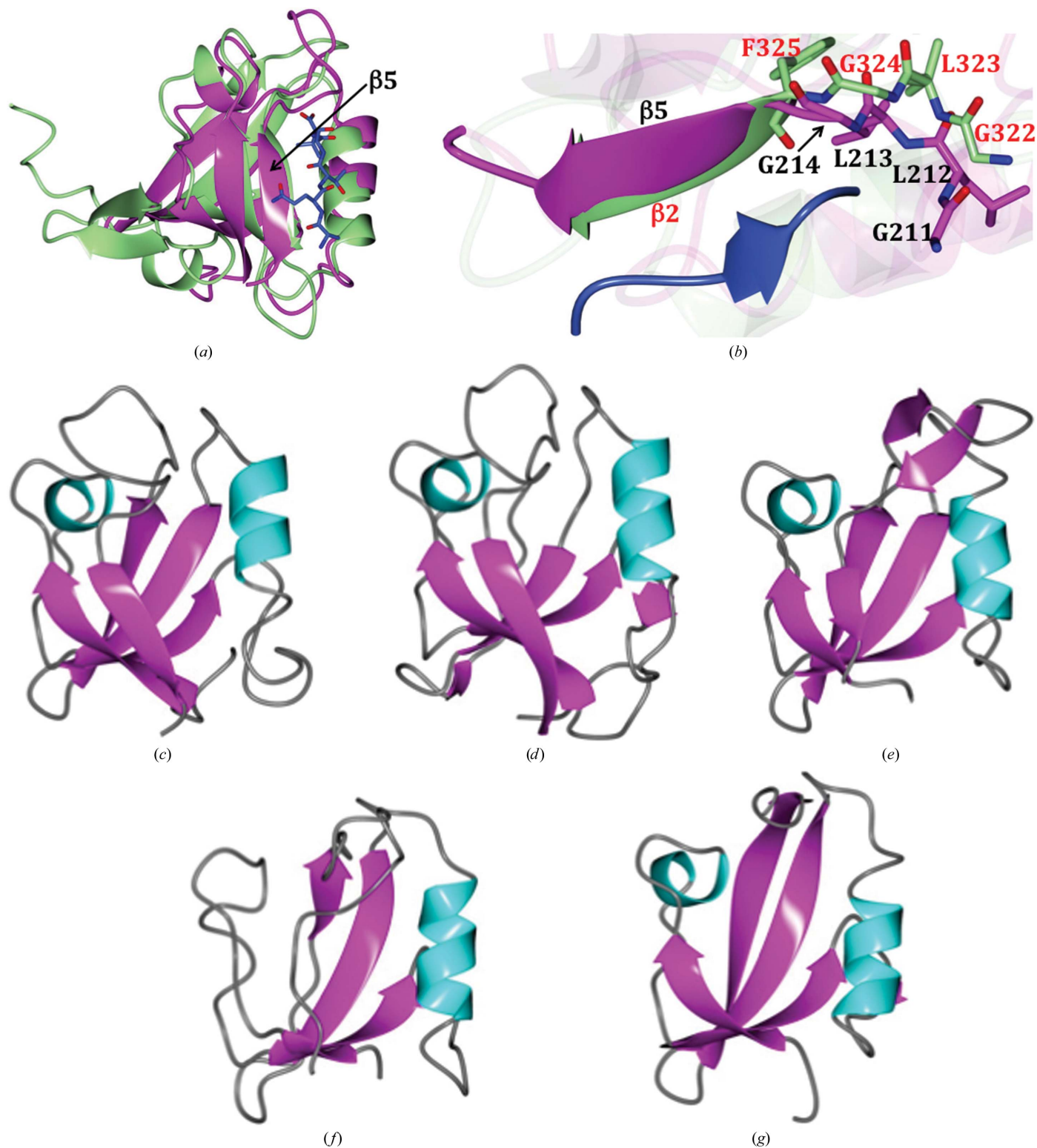
The C-terminal half of Nas2 constitutes a PDZ domain, while the N-terminal half has no predicted domain structure (Supplementary

Fig. S1a<sup>1</sup>). Nas2 directly interacts with the proteasomal ATPase subunit Rpt5, requiring the last three amino acids of Rpt5 for binding (Lee *et al.*, 2011). Since many PDZ domains bind to C-termini (Lee & Zheng, 2010), this suggests that the Nas2 PDZ domain is responsible for the interaction with Rpt5. Surprisingly, however, deletion of only the ultimate C-terminal residue of Rpt5 had little impact on Rpt5–Nas2 binding (Lee *et al.*, 2011). To gain a structural understanding of the interaction between Nas2 and Rpt5, we attempted to crystallize or co-crystallize Nas2 with the C-domain of Rpt5. Since no crystals were obtained, we created two truncated forms of Nas2 with the goal of minimizing the sequence around the PDZ domain. The truncated forms of Nas2 retained their ability to bind to the Rpt5 C-domain and showed only a modest reduction in affinity as measured using bio-layer interferometry (Supplementary Fig. S1b). Nas2LND produced well diffracting crystals after two months, enabling us to determine a structure comprised of amino acids Gln129–Leu220 in the asymmetric unit (Fig. 1). Nas2LND adopts a fold consisting of five  $\beta$ -sheets and two  $\alpha$ -helices commonly found amongst PDZ-domain structures (Fig. 1). N-terminal residues from cloning that spanned Gly115–Gly124 could be traced in the electron-density maps (blue in Fig. 1).

<sup>1</sup> Supporting information has been deposited in the IUCr electronic archive (Reference: HV5251).

However, residues between Gly124 and Gly129 were disordered and could not be modeled. Fig. 1 shows the N-terminal fragment Gly115–

Gly124 belonging to the same chain; however, we cannot exclude the possibility it is derived from a neighboring molecule in the crystal



**Figure 3**

(a) Superposition of Nas2LND (magenta) with a canonical PDZ domain (PDB entry 1be9, green). The peptide ligand for 1be9 is shown as blue cylinders.  $\beta$ -Sheet 5 of Nas2LND is indicated. Superposition of a canonical PDZ domain (PDB entry 1be9) with Nas2LND was conducted using *GESAMT* (Krissinel, 2012), which yielded an r.m.s.d. of 2.27 Å for 59 aligned residues. (b) Enlarged view of the  $\beta$ 5/ $\alpha$ 2 region of Nas2LND superimposed with 1be9. The peptide ligand for 1be9 is shown as a blue ribbon. The GLGF (red) motif of 1be9 and similar residues in front of Nas2LND  $\beta$ -sheet 5, GLLG (black), are indicated. (c–f) Superposition of specified regions of PDZ-domain homologs onto Nas2LND colored by secondary structure as in Fig. 1. (c) Nas2LND, (d) PDB entry 3rle (chain A, residues 7–104), (e) PDB entry 3id4 (chain A, residues 223–307), (f) PDB entry 3i1e (chain B, residues 3–85) and (g) PDB entry 3gdv (chain C, residues 279–410).

(Supplementary Fig. S2). Following refinement, recurring electron density was observed in two regions. The first was modeled as a disordered PEG 400 fragment obtained from the cryoprotectant (Supplementary Fig. S3a). The second region was observed between Lys119 and Lys120 and was assigned as a sulfate ion (Supplementary Fig. S3b).

### 3.2. Structural comparison with other PDZ domains

The structured residues of Nas2 were aligned with the human ortholog p27/PSMD9 (Fig. 2a). Several conserved residues are clustered on the surface of the PDZ domain (Figs. 2b and 2c). Interestingly, there is a group of identical hydrophobic residues covering the region between  $\alpha$ -helix 2 and  $\beta$ -sheet 5 (Figs. 2b and 2c), a region that is known to be the peptide-binding groove in other PDZ domains (Lee & Zheng, 2010; Fig. 3a). Similar to what was reported for GRASP55 (PDB entry 3rle), the groove was formed by the final, instead of the second,  $\beta$ -strand (Figs. 3a and 3b), indicating a similar circular permutation from a typical eukaryotic PDZ domain (Truschel *et al.*, 2011). At the entrance of this groove there are conserved charged residues. Besides the groove, there are other surface areas that appear to contain a cluster of conserved residues, maybe facilitating additional binding interactions as the residues do not appear to be structural.

To compare the structure of Nas2 PDZ with a typical PDZ domain that utilizes a GLGF motif for binding the C-terminus of other proteins (Lee & Zheng, 2010), we aligned the structure with PDB entry 1be9 (Doyle *et al.*, 1996). The GLGF motif is located before the  $\beta$ -strand 2 of 1be9. This compares to the region in front of  $\beta$ -strand 5 in Nas2LND owing to the altered  $\beta$ -strand arrangement (Figs. 3a and 3b). Interestingly, a similar motif is found in this region in Nas2LND (GLLG; Figs. 2a and 3b). Next, the structure of Nas2LND was also compared with the top structures obtained from a DALI search (Holm & Rosenström, 2010), and the coordinates were superimposed using GESAMT (Krissinel, 2012). Overall, the structure of Nas2LND is similar to these homologous structures as indicated from superpositions: r.m.s.d.s of 1.30 Å with PDB entry 3rle (chain A, residues 7–104; 87 residues; Truschel *et al.*, 2011), 1.30 Å with PDB entry 3id4 (chain A, residues 223–307; 74 residues; Li *et al.*, 2009), 1.68 Å with PDB entry 3ile (chain B, residues 3–85; 75 residues; Northeast Structural Genomics Consortium, unpublished work) and 1.68 Å with PDB entry 3gdv (chain C, residues 279–410; 72 residues; Sohn *et al.*, 2009). A side-by-side comparison of these structures is shown in Figs. 3(c)–3(f).

### 4. Conclusion

The 1.15 Å resolution crystal structure of the C-terminal region of Nas2 shows it contains a PDZ domain. Nas2 lacks the GLGF motif commonly found just prior to  $\beta$ -strand 2 in PDZ domains. This motif interacts with the carboxy-termini of PDZ-binding partners (Lee & Zheng, 2010). The absence is not surprising as the Nas2 structure shows that  $\beta$ -strand 5, instead of the common  $\beta$ -strand 2, contributes to the putative peptide-binding groove, causing a different loop arrangement. In front of  $\beta$ -strand 5 a similar sequence is present (GLLG). However, the role of this sequence in interactions with C-termini of Nas2-binding partners remains to be determined. In particular, the binding between Nas2 and Rpt5 does not appear to be affected by deletion of the Rpt5 C-terminal residue (Lee *et al.*, 2011). The reported Nas2 structure will provide the basis for further insights regarding the structure and function of Nas2 in proteasome assembly, as it will facilitate molecular docking of the tail of Rpt5 as well as

enabling the design of Nas2 mutants based on the putative binding region.

This work was supported by grants from the Johnson Cancer Research Center, the NIH-NCRR (5P20RR017708 and P20 RR016475) and NIH (8 P20 GM103420 and P20 GM103418). Use of IMCA-CAT was supported by IMCA through a contract with the Hauptman–Woodward MRI. Use of the APS was supported by the US Department of Energy (Contract No. DE-AC02-06CH11357). Publication of this article was funded in part by the Kansas State University Open Access Publishing Fund.

### References

- Adams, P. D. *et al.* (2010). *Acta Cryst.* **D66**, 213–221.
- Barrault, M.-B., Richet, N., Godard, C., Murciano, B., Le Tallec, B., Rousseau, E., Legrand, P., Charbonnier, J.-B., Le Du, M.-H., Guérois, R., Ochsenbein, F. & Peyroche, A. (2012). *Proc. Natl Acad. Sci. USA*, **109**, E1001–E1010.
- Beck, F., Unverdorben, P., Bohn, S., Schweitzer, A., Pfeifer, G., Sakata, E., Nickell, S., Plitzko, J. M., Villa, E., Baumeister, W. & Förster, F. (2012). *Proc. Natl Acad. Sci. USA*, **109**, 14870–14875.
- Bedford, L., Paine, S., Sheppard, P. W., Mayer, R. J. & Roelofs, J. (2010). *Trends Cell Biol.* **20**, 391–401.
- Chen, V. B., Arendall, W. B., Headd, J. J., Keedy, D. A., Immormino, R. M., Kapral, G. J., Murray, L. W., Richardson, J. S. & Richardson, D. C. (2010). *Acta Cryst.* **D66**, 12–21.
- Diederichs, K. & Karplus, P. A. (1997). *Nature Struct. Biol.* **4**, 269–275.
- Doyle, D. A., Lee, A., Lewis, J., Kim, E., Sheng, M. & MacKinnon, R. (1996). *Cell*, **85**, 1067–1076.
- Ehlinger, A., Park, S., Fahmy, A., Lary, J. W., Cole, J. L., Finley, D. & Walters, K. J. (2013). *Structure*, **21**, 753–765.
- Emsley, P., Lohkamp, B., Scott, W. G. & Cowtan, K. (2010). *Acta Cryst.* **D66**, 486–501.
- Evans, P. (2006). *Acta Cryst.* **D62**, 72–82.
- Evans, P. R. (2011). *Acta Cryst.* **D67**, 282–292.
- Evans, P. (2012). *Science*, **336**, 986–987.
- Evans, P. R. & Murshudov, G. N. (2013). *Acta Cryst.* **D69**, 1204–1214.
- Funakoshi, M., Tomko, R. J. Jr, Kobayashi, H. & Hochstrasser, M. (2009). *Cell*, **137**, 887–899.
- Groll, M., Ditzel, L., Löwe, J., Stock, D., Bochtler, M., Bartunik, H. D. & Huber, R. (1997). *Nature (London)*, **386**, 463–471.
- Holm, L. & Rosenström, P. (2010). *Nucleic Acids Res.* **38**, W545–W549.
- Kabsch, W. (2010a). *Acta Cryst.* **D66**, 125–132.
- Kabsch, W. (2010b). *Acta Cryst.* **D66**, 133–144.
- Kaneko, T., Hamazaki, J., Iemura, S., Sasaki, K., Furuyama, K., Natsume, T., Tanaka, K. & Murata, S. (2009). *Cell*, **137**, 914–925.
- Karplus, P. A. & Diederichs, K. (2012). *Science*, **336**, 1030–1033.
- Krissinel, E. (2012). *J. Mol. Biochem.* **1**, 76–85.
- Lander, G. C., Estrin, E., Matyskiela, M. E., Bashore, C., Nogales, E. & Martin, A. (2012). *Nature (London)*, **482**, 186–191.
- Langer, G., Cohen, S. X., Lamzin, V. S. & Perrakis, A. (2008). *Nature Protoc.* **3**, 1171–1179.
- Lee, H.-J. & Zheng, J. J. (2010). *Cell Commun. Signal.* **8**, 8.
- Lee, S. Y.-C., De La Mota-Peynado, A. & Roelofs, J. (2011). *J. Biol. Chem.* **286**, 36641–36651.
- Le Tallec, B., Barrault, M.-B., Guérois, R., Carré, T. & Peyroche, A. (2009). *Mol. Cell*, **33**, 389–399.
- Li, X., Wang, B., Feng, L., Kang, H., Qi, Y., Wang, J. & Shi, Y. (2009). *Proc. Natl Acad. Sci. USA*, **106**, 14837–14842.
- Long, F., Vagin, A. A., Young, P. & Murshudov, G. N. (2008). *Acta Cryst.* **D64**, 125–132.
- Matthews, B. W. (1968). *J. Mol. Biol.* **33**, 491–497.
- McCoy, A. J., Grosse-Kunstleve, R. W., Adams, P. D., Winn, M. D., Storoni, L. C. & Read, R. J. (2007). *J. Appl. Cryst.* **40**, 658–674.
- McNicholas, S., Potterton, E., Wilson, K. S. & Noble, M. E. M. (2011). *Acta Cryst.* **D67**, 386–394.
- Nakamura, Y., Umehara, T., Tanaka, A., Horikoshi, M., Padmanabhan, B. & Yokoyama, S. (2007). *Biochem. Biophys. Res. Commun.* **359**, 503–509.
- Park, S., Li, X., Kim, H. M., Singh, C. R., Tian, G., Hoyt, M. A., Lovell, S., Battaile, K. P., Zolkiewski, M., Coffino, P., Roelofs, J., Cheng, Y. & Finley, D. (2013). *Nature (London)*, **497**, 512–516.
- Roelofs, J., Park, S., Haas, W., Tian, G., McAllister, F. E., Huo, Y., Lee, B.-H., Zhang, F., Shi, Y., Gygi, S. P. & Finley, D. (2009). *Nature (London)*, **459**, 861–865.

- Saeki, Y., Toh-e, A., Kudo, T., Kawamura, H. & Tanaka, K. (2009). *Cell*, **137**, 900–913.
- Sohn, J., Grant, R. A. & Sauer, R. T. (2009). *Structure*, **17**, 1411–1421.
- Takagi, K., Kim, S., Yukii, H., Ueno, M., Morishita, R., Endo, Y., Kato, K., Tanaka, K., Saeki, Y. & Mizushima, T. (2012). *J. Biol. Chem.* **287**, 12172–12182.
- Tian, G., Park, S., Lee, M. J., Huck, B., McAllister, F., Hill, C. P., Gygi, S. P. & Finley, D. (2011). *Nature Struct. Mol. Biol.* **18**, 1259–1267.
- Truschel, S. T., Sengupta, D., Foote, A., Heroux, A., Macbeth, M. R. & Linstedt, A. D. (2011). *J. Biol. Chem.* **286**, 20125–20129.
- Weiss, M. S. (2001). *J. Appl. Cryst.* **34**, 130–135.